Journal of Materials Science and Nanotechnology
Volume 12 | Issue 2
ISSN: 2348-9812

Research Article Open Access

Theoretical Studies of the Electronic and Thermoelectric Properties of $PrIn_3$ and $NdIn_3$ in Cubic Phase

Qasimullah[1], M Irfan[1], WU Rahman[2,*], Nasir Shehzad[3], M.Ilyas[4] and Hussain Ahmad[5]

[1]Qurtuba University of science and information technology Peshawar, Pakistan
[2]School of Physics and Electronics, Hunan University, Changsha 410082, PR China
[3]Hunan Provincial Key Laboratory of High-Energy Scale Physics and Applications, School of Physics and Electronics, Hunan University, Changsha 410082, PR China
[4]Institute of Physics, Gomal University, Dera Ismail Khan, 29220, Khyber Pakhtunkhwa, Pakistan
[5]Department of physics, Abdul Wali Khan University Mardan ,23200, Pakistan

[*]**Corresponding Author:** WU Rahman, School of Physics and Electronics, Hunan University, Changsha 410082, PR China, Tel.: +8618207425602, E-mail: waheed2233@hnu.edu.cn

Citation: Qasimullah, M Irfan, WU Rahman, Nasir Shehzad, M.Ilyas, Hussain Ahmad (2024) Theoretical Studies of the Elec tronic and Thermoelectric Properties of PrIn3 and NdIn3 in Cubic Phase, J Mater Sci Nanotech nol 12(2): 202

Received Date: June 10, 2024 **Accepted Date:** July 10, 2024 **Published Date:** July 14, 2024

Abstract

The electronic and thermoelectric properties of AB_3 (A =Pr, Nd and B=In) materials (crystallizing in the cubic structure) having space group Pm-3m (221) are studied using B3PW91 hybrid functional through the Full-Potential Linear Augmented Plane Wave (FP-LAPW) approach within the framework of Density Functional Theory (DFT). The calculated lattice parameters for $PrIn_3$ and $NdIn_3$ are 4.5668 Å and 4.5539 Å respectively. Electron-electron correlation effect is due to the 4f orbitals present in these materials and therefore, with the use of B3PW91 hybrid functional, band structure and density of states are calculated. When analyzing electron charge density, these materials showed a stronger ionic character. Band structure and density of state analysis confirms the metallic nature of the materials. Using the semi-empirical Boltzmann approach implemented in the BoltzTraP code, the thermoelectric parameters, such as Seebeck coefficient, figure of merit, electrical conductivity per relaxation time, and electronic thermal conductivity per relaxation time as a function of chemical potential, were computed at 500 K temperature gradient. $PrIn_3$ showed highest Seebeck coefficient value, 50.68μV/K among these compounds. The peak value of electrical conductivity per relaxation time and electronic thermal conductivity per relaxation time among these compounds is calculated for $NdIn_3$ is 2.43 x 1020 1/Ωms and 22.50×1014 W/mKs.

Keywords: DOS; Seebeck coefficient; Figure of merit; Chemical potential; Band structure; Electron charge density

Introduction

Rare earth intermetallic play a distinctive role in a variety of technological applications, particularly in the realm of permanent magnets, and this is true from both a theoretical and practical perspective. These materials are identified to have heavy fermions, valence fluctuations, Kondo lattices, permanent-magnet materials, spin glasses, and random anisotropy systems. It is pointed out that in this vast number of materials there is an ideal chance of establishing which of several second-order terms are effective in determining structural stability dealing with intermetallic, the rare earths (RE) based intermetallic have promising of cubic crystal structure more favorable for industrial applications. [1-3]. The general chemical formula of the binary intermetallic compounds is AB_3 where A=Pr, Nd and B=In. The materials have space group Pm-3m No 221 and atomic position A is at (0, 0, 0,) and B is located at (0, ½, ½) [4]. Schottky anomalies have been observed and analyzed in specific heat measurements on $Celn_3$, $Prln_3$. Susceptibility studies have led to the determination of the ground state levels in praseodymium compounds [5]. Diepen *et al.* [6] investigated heat capacities of AB_3 (A= Pr, Nd and B= In) systems which have been found between 7 and 300 K. The $LaIn_3$ calculations is adjust in a Debye curve of ϑ =170 K. The magnetic properties of the AB_3 (A = Pr, Nd and B=In) compounds has been experimentally studied in the recent past comparing $LaIn_3$ to the other $LnIn_3$ compounds, $LaIn_3$ has a lower electronic specific heat coefficient (5.3 mJ/(K^2.mol)) and a higher gamma value (120 mJ/(K^2.mol)) than the other $LnIn_3$ compounds. $SmSn_3$, $EuSn_3$, and $GdSn_3$ exhibit AFM transitions for the $LnSn_3$ series at temperatures T_N = 12 K, 36.5 K, and 16.5 K, respectively, based on magnetic susceptibility tests, where it was found that the majority of the lanthanide $LnIn_3$ compounds are AFM at low temperatures Sanchez *et al.* [7]. Onuki and Settai used Mössbauer resonance to determine the electrical and magnetic qualities of $LnSn_3$ compounds (Ln = La, Ce, Pr, Nd, Sm, Eu, Gd, Yb) [8]. The heat capacities were studied between 7 K and 300 k in a calorimeter of the adiabatic type [9] With the exception of $EuSn_3$ and $YbSn_3$, $LnIn_3$ (In = Sn) exhibits the typical lanthanide contraction over the era induced by the insertion of another electron into the 4f orbital. The atom shrinks in size compared to its earlier iteration as a result of the increased nuclear charge's stronger attractive effect on the electron cloud. Because europium and ytterbium atoms are in a divalent (2+) and the other are in a trivalent (3+) ionic state, the lattice parameters of $EuIn_3$ and $YbIn_3$ are larger [10]. The Fermi surface of $PrIn_3$ is almost the same as that of the non-f reference material, $LaIn_3$. The Fermi surfaces and cyclotron masses of $PrIn_3$ are in the range of 0.3 m_0 to 1 m_0, which are twice larger than those of $LaIn_3$ [11]. Magnetoresistance and de Haas-van Alphen (dHvA) effect in both the antiferromagnetic and paramagnetic states of $NdIn_3$ measured. Many dHvA branches are detected in the dHvA experiments. Among them, a nearly spherical Fermi surface in the paramagnetic state, which corresponds to a band 7-electron Fermi surface of the non-4f reference compound $LaIn_3$, is changed in the antiferromagnetic state into a multiply connected Fermi surface with necks. The cyclotron masses of $NdIn_3$ are in the range of 0.30m_0 to 1.05m_0, which are twice as large as those of $LaIn_3$ [12]. The specific heats of RIn_3 (R = La, Ce, Pr, Nd, Sin, Gd, Tb and Ho) is measured between 0.2 and 2.2 K. The electronic specific heat coefficients are found to be enhanced for magnetic RIn_3 [13]. $CeIn_3$ possesses a large electronic specific heat coefficient -y 130mJ/K^2 mol at low temperature, indicating a heavy-electron system. Recently, the dHvA effect of $PrIn_3$, $NdIn_3$, $SmIn_3$, $LaIn_3$, $CeIn_3$ and $GdIn_3$ are measured. From the results of our dHvA experiments and band calculations done by Hasegawa *et al.* [14]. Therefore, in this manuscript, the semi-classical Boltzmann method was applied to the BoltzTraP package, enabling the determination of thermoelectric properties such as thermal conductivity, the Seebeck coefficient, thermal conductivity and figure of merit (ZT). The Seebeck Coefficient for NdIn3ranges from 11.96 μV/K to 8.08 μV/K within the energy range of 0.00 eV to -0.02 eV, whereas PeIn3 exhibits a Seebeck Coefficient of -11.99 μV/K. In the N-type region, the maximum Seebeck Coefficients for these materials are -0.35 to 0.57 μV/K for KAlTe2 and 5.5 to 6.7 μV/K for KInTe2, respectively. Strongly correlated electronic systems include f-block elements and their compounds are more attractive in condensed-matter physics because of their numerous practical applications, properties and fascinating physics. Some materials have exceptional magnetic, electrical, optical, and mechanical properties that depend on electron-electron correlation phenomena [15-17]. The history of the correlated electronic materials began in 1930's of prior eras. Theoretical concepts were initially created before there was a lot of actual effort in this field. Wigner introduced the key ideas using the idea of an electron crystal lattice [18]. RX_3 systems (R= Rare-earth and X= Pb, In, Tl) with space

group is Pm-3m (221) have been explored experimentally and theoretically by many researchers due to the phenomena of magnetism, superconductivity, crystal field effect, and kondo type behaviors. Some of these systems exhibit the coexistence of large, temperature-dependent paramagnetic susceptibility and superconducting transition temperature. The transition temperatures of $LaPb_3$ and $LaTl_3$ compounds are greater than $LaIn_3$ but $LaIn_3$ has a transition temperature of little more than 1 K. Lead atoms are in quadrivalent ionic state, but indium or thallium atoms are in a trivalent ionic state. The valences of the lanthanide in RX_3 compounds can be estimated using the lattice constant measuring method. For pure lanthanides, Ln^{2+} has a nearly 10% greater lattice constant than Ln^{3+} [19-24]. Due to intriguing qualities, including large melting points, ductility, best physical properties, lanthanides based intermetallic materials are desirable materials for research. Additionally, rare-earth intermetallic are superior to other metals as materials for the development of commercial aviation turbines [25-26]. Due to the fact that RX_3 compounds crystallize in a variety of crystal forms with varying atomic coordination and bond-length values, the rare-earth in several practical applications, intermetallic RX_3 exhibit outstanding physical qualities [27]. Rare-earth intermetallic put in a noteworthy performance in numerous technological applications. This is true both conceptually and practically. RX_3 (R= Rare-earth and X = Pb, In) with a cubic crystal structure are preferred for industrial applications [28-29]. RIn_3 and RSn_3 chemicals exhibit lanthanide contraction across the whole series. RX_3 compounds are easy to form in a single crystal due to their proper coherent melting. In contrast, X can be replaced by a member of group IIIA, IVA, or a transition metal to create a huge variety of RX_3 intermetallic compounds. When X is changed, these compounds may take on a broad variety of forms (X might be (In, Tl, Pb), of these compounds are straightforward to make since they melt identically. Since cubic symmetry crystallizes in many RX_3 compounds, it is preferred to lower symmetry for superconductivity and can be further boosts ductility in the aerospace industry [30-33].

Method of Calculations

The bonding in these systems may be properly described by quantum mechanical methods. Nevertheless, current computing resources cannot resolve problems involving systems with more than a few atoms, making correct answers hard to get. Using approximate theoretical approaches, such as first principle or semi-empirical computations, is one method that can help us tackle these issues. First principles, also known as ab initio, are theoretical frameworks that begin with the proven fundamental laws of physics and do not rely on or make any presumptions, such as empirical models and parameter fitting. They don't rely on or make any assumptions. Using these methods is intended to get a clear description of the system's electronics wave function. The electrical structure of matter is studied using Density functional theory (DFT), a quantum mechanical modelling technique. Instead of utilizing the many-body wave function to describe the features of the many-body system, this DFT uses the functional rely on electron density of the system [34]. DFT has emerged as a potent theoretical tool to study the chemical and physical properties of crystal materials throughout the past century. On DFT, several researchers have worked. Over the past 20 years, it has been a commonly used instrument in the majority of chemical and material science domains. Because of its precision and low computing cost, DFT has gained popularity [35]. The density functional theory (DFT) framework, in combination with the full-potential Linearized Augmented Plane Wave (FP-LAPW) method, has been implemented using the WIEN2k package [36], to examine the electronic nature of $PrIn_3$ and $NdIn_3$. In order to determine the structural features, the local density approximation (LDA) was used to represent the exchange-correlation energy [37] and the generalized gradient approximation of Perdew et al. [38]. A straightforward method for enhancing calculations of numerous molecular parameters, including as optimization energies, bond lengths, and vibration frequencies, which frequently suffer from poor description by straightforward ab initio functionals, is hybridization with Hartree-Fock (HF) exchange, also known as exact exchange. The Hartree-Fock exact exchange functional and any number of exchange and correlation explicit density functionals are often linearly combined to create a hybrid exchange- correlation functional. The hybrid functionals implemented in wien2k are classified in to two types: full hybrid functionals and onsite hybrid functionals. For solid the full hybrid functional is computationally very expensive. On-site method as cheap as LDA/GGA. B3PW91 hybrid functionals are used to investigate the band structure and DOS

for metallic materials [39]. The thermoelectric coefficients were determined by solving the Boltzmann transport properties using a constant relaxation time, the rigid band approximation, and first-principles calculations [40].

Results and Discussion

Electronic Charge Density

The electron charge density provides a thorough analysis of the bonding factor in the material and a significant representation of the majority of bonding. Similar to DFT, we deal with the material properties and identify the cell structure in order to estimate the electron charge density. The electron charge density is an analysis tool that can be used to better understand the structure of a material and how its atoms are bonded. This is achieved by looking at the distribution of electrons among individual atoms, which can determine whether bonding is covalent or ionic in nature. By understanding this relationship, scientists can gain a clearer view of the bulk bonding within a compound [41]. Researchers can quantify the spacing between the ions in the lattice and distinguish between different ions using data taken from the electron density plots. Researchers can quantify the spacing between the ions in the lattice and distinguish between different ions using data taken from the electron density graphs. Figures 3. 1 clearly show the present of ionic bonds which is present in all atoms. Nd makes strong ionic bond with In atom, because Nd electronegativity is higher than Pr. A useful tool for explaining highly linked electrical systems is HF. B3PW91 has the ability to effectively address these systems in lanthanides [42]. Similarly, to achieve better results in the HF computations, the precise exchange α is chosen to 0.2 eV. The plane wave basis functions are determined via RMTKmax¼8.00 using 286 k-points. Non-shifted meshes with 1000 k points are utilized for the electronic computations, while 10000 k points are used for the transport calculation. Using the BoltzTraP code, the calculated electronic structures are utilized to examine related to thermoelectric parameters [43].

Band Structure

One of the most fundamental parameters that defines a compound which has many physical properties would be its band gap. The band gap of a material is responsible for a complete measurement of different physical properties like optical, mechanical, optoelectronic and thermoelectric of the material. Because, the information of the electronic band structure of a material is important for its future technical implementation in various devices [44]. Electronic structure of a material plays an important role in determining their physical properties, particularly, the thermoelectric properties. The methods of determining electronic structure have developed swiftly during the last quarter of the twentieth century, particularly by the Density functional theory (DFT), due to the development of computer skills and the computation power. There are great numbers of DFT-based computational programs which can be accurately used to compute electronic structure of materials. Self-consistent field (SCF) computations are performed for the study of electronic band structures of these compounds as described earlier [45-47]. Exact value of the band gap and its nature could be inferred from the band structure. The negative energy states correspond the valance band while the positive energy states correspond to the conduction band and Ef represent the Fermi energy level that coincide with the valance band edge at the zero energy states. In Figures 3.2 the energy range from -14 eV to 8 eV which is observed along the high symmetry directions in the first Brillouin zone. At zero pressure, the bands at the Fermi level for materials $PrIn_3$ and $NdIn_3$ are extremely similar along all high symmetry lines. The different colors in the band structure represent the energy states. Which is clearly described in DOS. At 0.0 eV, the Fermi energy level between the valence band and conduction band is assumed. The Figures 3.2 also show that in all compounds, the symmetry point R, Γ, X and M is where the states overlap. No bandgap is observed for these compounds, hence all of them are metallic. The present study about $PrIn_3$ and $NdIn_3$ intermetallic materials show that there is no band gap between conduction and valance band make these compounds favorable for attaining novel materials properties.

Density of States

The density of states (DOS) of a system in solid state and condensed matter physics explains the number of states per energy per volume that will be filled by the system for each level of energy. The curves of density of states explained the contribution to the structure of the bands and the existence of the bonds. Band structure and the type of bonds are both explained by density of states. Figures 3.3 displays the total density of states (TDOS) as well as the partial density of states (DOS) for $PrIn_3$ and $NdIn_3$ materials. The density of states plots is shown in the Figures 3.3, where the negative energy states corresponds to the valance band while the positive energy states correspond to the conduction band and Ef represent the Fermi energy level that coincide with the valance band edge at the zero energy states. Figures 3.3 displays the results of the TDOS and PDOS computations for the $PrIn_3$ and $NdIn_3$ materials. The valence band and conduction band are mainly contributed by Pr/Nd and In for these materials. From the total density of states plots in Figure 3.3 one can't determine which states of Pr/Nd and In are contributing towards the conduction and valence band edges, this information is obtained from the plots of partial density of states given in Figures 3.3 which allow us to learn how frequently each state occurs in atoms conduction band and valence band. Pr-f, Pr-d, Nd-f and Nd-d make up the majority of the contribution at the Fermi level E_f and specifies the contribution and bonding at the Fermi level. The associated bonding is with the states In-s at the $E_{f,}$ while rest of the states have negligible contibution.

Seebeck Coefficient

The Seebeck effect allows creation of voltage on the basis of the temperature difference. The magnitude of the effect is represented by the Seebeck parameter, S, given by the equation $S = V/\Delta T$ where V is Voltage and ΔT is Temperature difference. When two different conductors are kept at different temperatures, the electrons on the hot end have high thermal energy than the electrons on the cold end. Therefore, electrons will flow towards the colder end. This net accumulation of electrons at the colder end gives a potential difference across the conductor, with the cold end being the negative. The materials with high Seebeck coefficient will have high Figure of merit that means greater capability to convert waste heat into useful electrical energy [48]. Different parameters are used to understand the thermoelectric phenomena. The most fundamental among these parameters is Seebeck coefficient which tells about the response of material to the applied temperature gradient. The value of Seebeck coefficient is negative for n- doped and is positive for p-doped. Chemical potential is defined as the concentration of the charge carrier in a material is the doping level of material. Chemical potential is important factor for enhancing thermoelectric nature. The plot of Seebeck coefficient against chemical potential for rare-earth intermetallic compounds AB_3 (A=Pr and Nd, B=In) are shown in the Figures 3.4 The figure shows that the highest Seebeck coefficient for the $PrIn_3$ and $NdIn_3$ in spin calculations in the p-type region 50.68 μV/K and 52.10 μV/K, respectively as shown in Figures 3.4 In the n-type region maximum value of Seebeck Coefficient for the same order of compound under study are -53.79 μV/K, -34.54 μV/K respectively. All the calculations are carried out at 500 K temperature. From the figure it is clear for all the compounds under study the maximum value of Seebeck coefficient for n-type and p-type region at the chemical potential of 0.02 eV to -0.02 eV.

Electrical Conductivity

Electrical conductivity is the movement of electrical charge in a substance. Materials having large electrical conductivity will be the best thermoelectric performers. A high electrical conductivity is necessary to minimize the heating of the conductor which is produced due to the passage of electric current (Joule heating). The greatest thermoelectric materials do, however, require a lot of electrically conductive components because of their high efficiency. Charge carriers in metallic compounds are electrons, but in semiconductors, holes and electrons are in charge. The fact that the materials under test are metals makes electrical conduction by electrons easier to calculate. For a material to have thermoelectric qualities, its electronic structure is essential, and free carriers are superior conductors. Figure 3.5 illustrates the relationship between electrical conductivity and chemical potential in spin calculations for the rare-earth intermetallic AB_3, where A=Pr and Nd, B=In. Electrical conductivity is expressed in these computations in units of order 10^{20} 1/Ωms. In p-type region maximum value of electrical conductivity for PrIn3 and Nd-

In3 are 2.10×10^{20}1/Ωms and 2.43×10^{20}1/Ωms respectively. In type minimum value of (σ/τ) for are 0.99×10^{20}1/Ωms and 1.16 $\times10^{20}$1/Ωms respectively.

Electronic Thermal Conductivity per Relaxation Time (κ/τ)

Thermal conductivity is significantly affected by the presence of electron-hole pairs in semiconductor materials. it can be expressed as k = ke + kh, where ke is associated with electron vibrations, and kh corresponds to hole vibrations. In semiconductors, thermal conductivity is attributed to electron-hole pairs, while in metals, it's predominantly driven by free charge carriers or electrons. [48-51]. Thermal conductivity is the transport of heat energy through a conductor as a result of temperature gradient from the direction of high temperature to lower. In crystals, heat is conducted through free electrons and lattice vibrations.

In semiconductors heat is conducted through lattice vibrations while in metals it takes place through free electrons [52]. The heat-flow measurements through the material when applying the temperature gradient are thermal conductivity. The thermal conductivity of the heat flow of the material is caused by phonemic vibrations and free electrons. The lattice part, however, contributes mainly to thermal conductivity in semiconductors, while free electrons contribute significantly to thermal conductivity in metals. The disadvantage of the BoltzTraP code is that the electronic component of thermal conductance can be determined, but thermal grid cannot be calculated. The plot of thermal conductivity per relaxation time (κ/τ) against chemical potential for AB3 (A=Pr, Nd and B=In) at 500 K temperature are shown in Figures 3. 6.

From the figure it is cleared that when the chemical potential increases from Fermi level i.e 0 μ(eV) on either side the (κ/τ) increases. It is realized that for the higher values of chemical potential (κ/τ) is maximum for n-type and p type region. For the compound under study the maximum value of (κ/τ) is in p-type region as compared to n-type region which show significant response of (κ/τ) in p-type region compared to n-type region. The peak value of (κ/τ) for $PrIn_3$ and $NdIn_3$ in p type region in spin calculations 28.3×10^{14}W/mKs, 22.50×10^{14}W/mKs and in n-type are 13.78×10^{14}W/mKs and 15.78×10^{14}W/mKs, respectively. Figure of Merit A parameter called the figure of merit is used to gauge a material's thermoelectric efficiency. The efficiency of the thermoelectric effect will increase with the merit Figure. The theoretical framework that is connected to the high Seebeck coefficient specifies the theoretical boundary of surveying the yield of thermoelectric materials. A material's ZT is an important boundary to understand a compound's productivity. Numerically it is represented as $ZT = S^2\sigma T/\kappa$, where S, σ, κ and T are those parameters which is explain in terms of Seebeck coefficient, electrical conductivity, thermal conductivity and the temperature and also counts the performance of the given thermoelectric boundaries [53-55].

High-value ZT materials are needed for industrial applications. ZT values greater than unity is known to be incredibly powerful for thermoelectric applications. Despite the fact that thermoelectric research has increased recently, scientists are still having trouble coming up with materials that may take the place of the methods used to generate energy today [56-58]. Figures 3.7 shows the curve of ZT against chemical potential for the rare-earth AB_3 (A=Pr, Nd and B=In) at 500K temperature. The peak ZT value for each of the compounds under study $PrIn_3$ and $NdIn_3$ is depicted as being close to the Fermi level in the picture. This means that n-type doping is a better option for materials with superior thermoelectric capabilities than n-type doping. $PrIn_3$ and $NdIn_3$ each have a peak ZT value in the figure of 0.016 and 0.014 respectively. We can see that the highest value of figure of merit is 0.016 for $PrIn_3$.

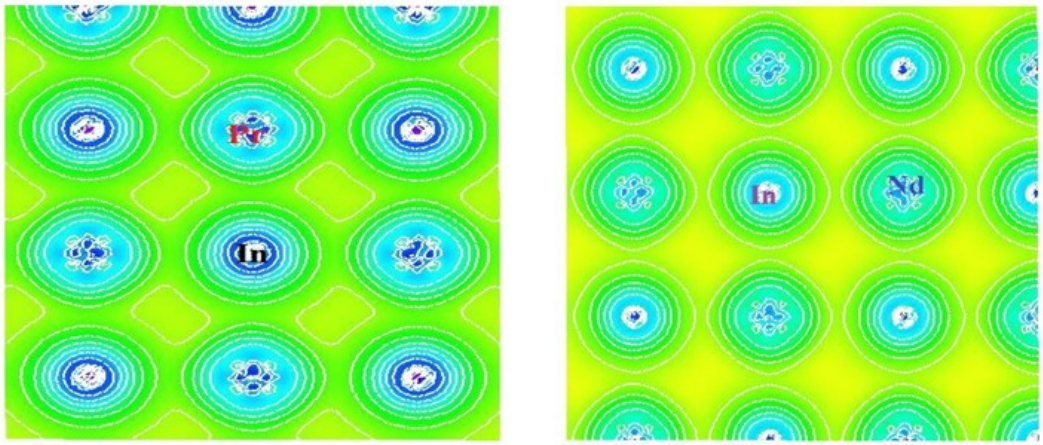

Figure 3.1: The electronic charge density of $PrIn_3$ and $NdIn_3$

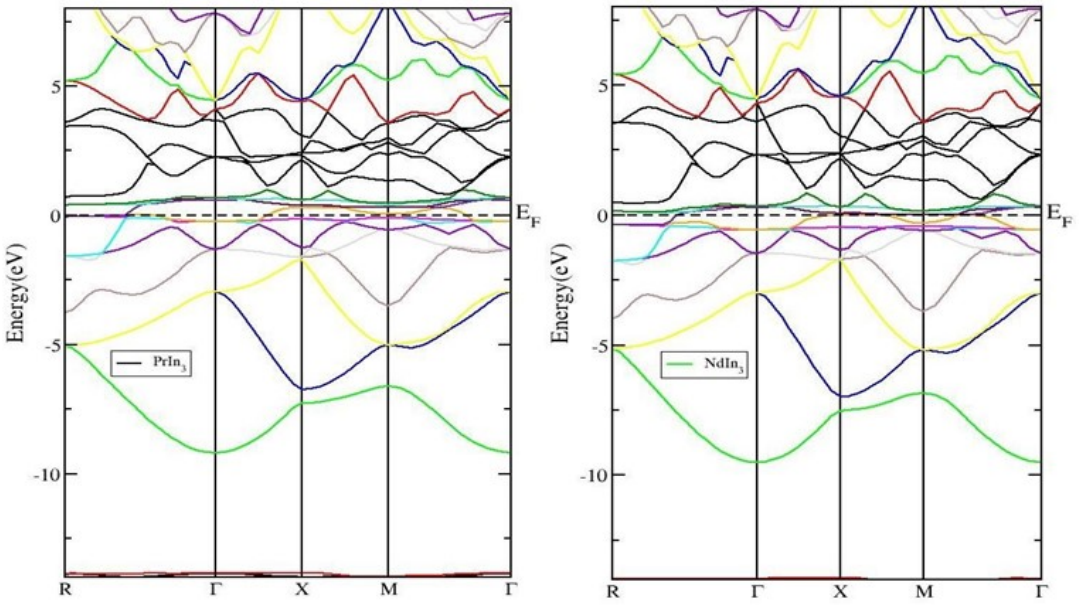

Figure 3.2: The band structure of $PrIn_3$ and $NdIn_3$

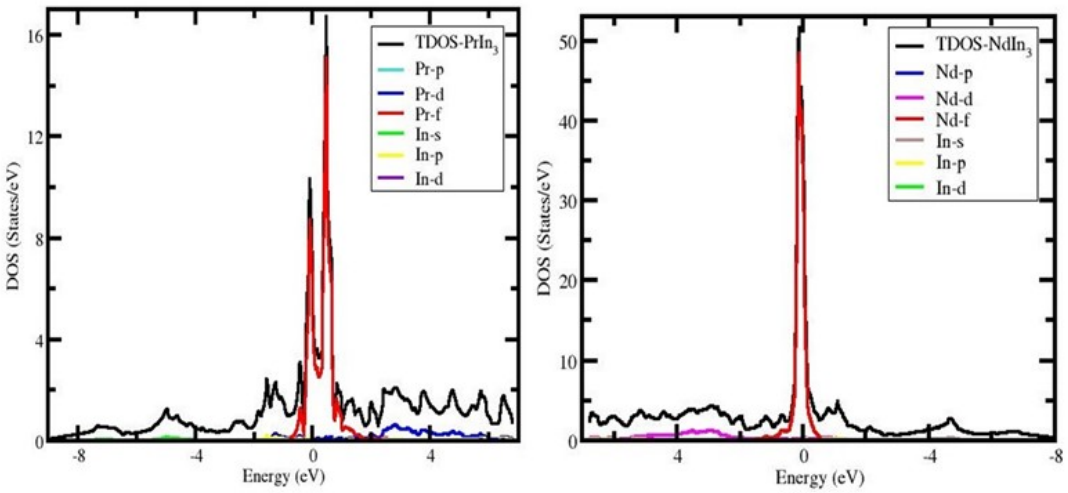

Figure 3.3: The density of states of $PrIn_3$ and $NdIn_3$

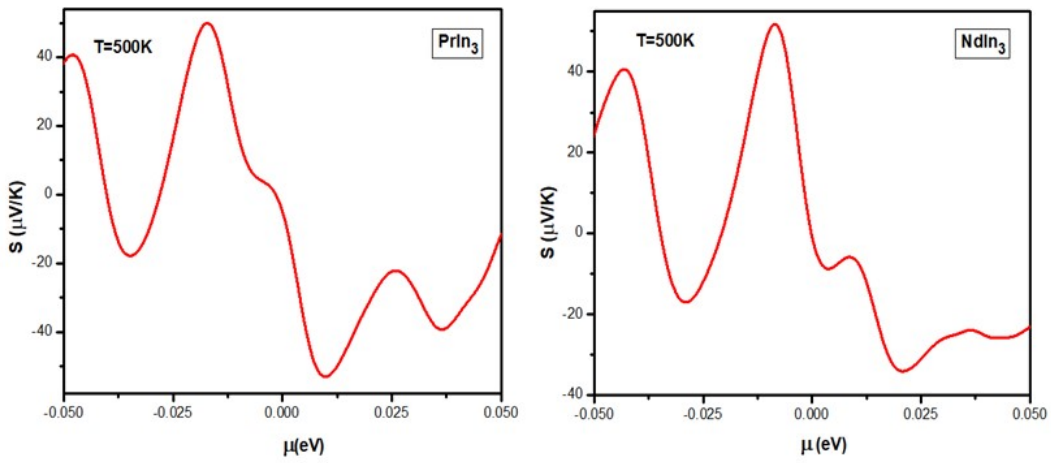

Figure 3.4: The Seebeck coiefient of $PrIn_3$ and $NdIn_3$

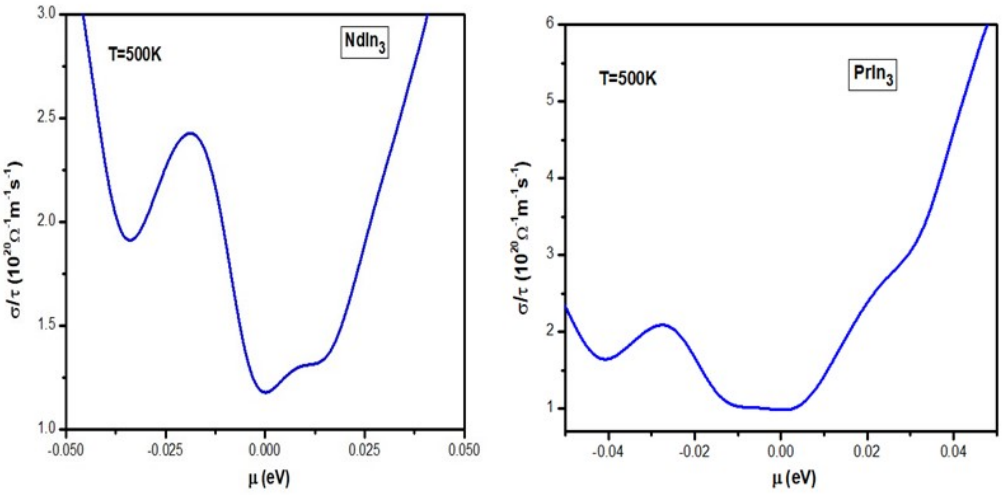

Figure 3.5: The electrical conductivity of $PrIn_3$ and $NdIn_3$

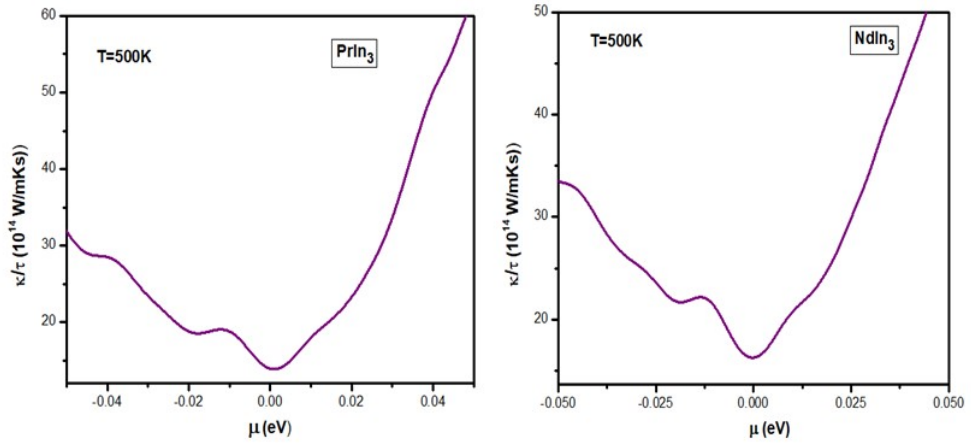

Figure 3.6: The thermal conductivity of $PrIn_3$ and $NdIn_3$

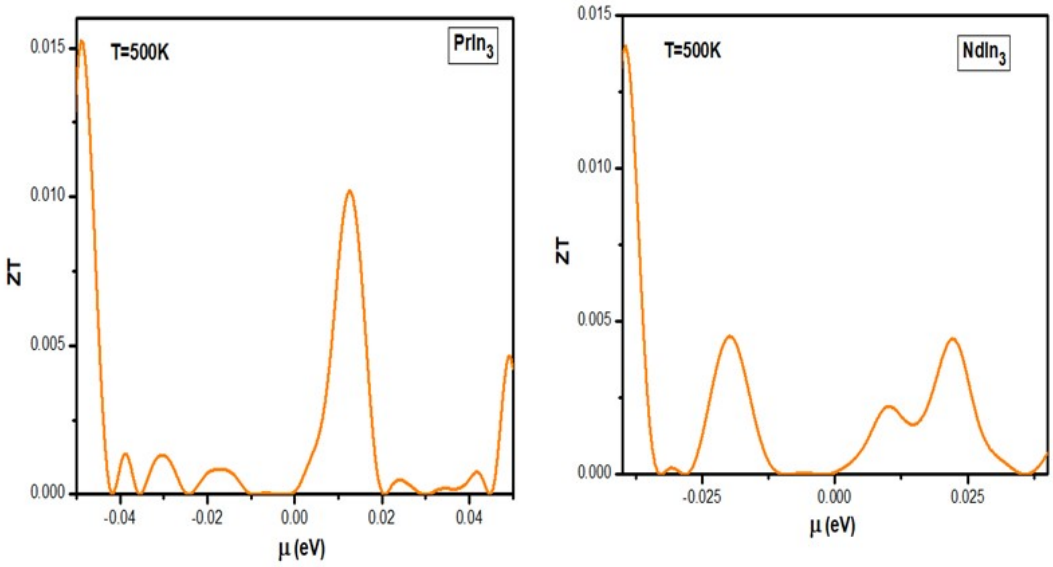

Figure 3.7: The Figure of $PrIn_3$ and $NdIn_3$

Summary and conclusion

The optimized lattice parameters are obtained using generalized gradient approximation based on density functional theory. The self-consistent calculation is performed with B3PW91 hybrid functional implemented on WIEN2K package to generate the band structure and density of states for these materials. From the band structure it is observed that the valence band and conduction band overlap at the Fermi level, which shows the metallic nature of these compounds. The TDOS and partial density of state plots are also observed. The maximum contribution in TDOS is due to 4f state while other states have negligible contributions. The electronic charge density in 100 planes indicate these compounds have stronger ionic bond. The BoltzTraP code is link with the WEIN2K code to determine the thermoelectric properties. $PrIn_3$ has highest Seebeck coefficient value, 50.68 μV/K among these compounds. The peak value of electronic thermal conductivity per relaxation time of $NdIn_3$ is 22.50×1014 W/mKs among these compounds. Electronic properties of these materials are investigated on the basis of spin polarized electronic band structure, total and partial density of states. These compounds have 4*f* orbitals and hence strong electron-electron correlation effect is expected, therefore, the electronic properties are also calculated with the B3PW91 hybrid functional and the effect of B3PW91 hybrid functional on the density of states is discussed in details. Spinning band occurs due to GGA's inability to correctly handle f-state, La f-state manifests at the Fermi level. We employ HF B3PW91 to get over this issue and localize the f-state electrons. By employing HF B3PW91, the f-state was correctly localized. Transport properties of these materials are calculated at the first time. The moderate values of figure of merit obtained for these materials indicate that these materials have applicability where small values of thermoelectric efficiency are required and higher values can harm the process but need experimental verification.

Acknowledgement

Not applicable

Conflicts of Interests

The authors declare that there is no complicit of interest regarding the publication of this paper

Data and Code Availability

The data and code availability not applicable

Supplementary information

Additionally, supplementary information not applicable

Ethical Approval

This research did not involve human participants, animals or sensitive data requiring ethical approval.

References

1. KNR Taylor (1971) Intermetallic rare-earth compounds, Advances in Physics, 20: 551-660,

2. JA Abraham, G Pagare, SP Sanyal (2015) Ab-initio Calculations of Structural, Electronic Elastic and Mechanical Properties of REIn3 and RETl3 (RE= Yb & Lu) Intermetallic Compounds, Advanced in Physics Theories and Applications, 45: 66-71.

3. K Purcell, D Graf, T Ebihara (2015) High Pressure Transport Studies of NdIn3," APS March Meeting Abstracts, 2015: G29-004.

4. F Birch (1947) Finite elastic strain of cubic crystals, Physical Review, 71: 809.

5. P Lethuillier, J Pierre, K Knorr, W Drexel (1975) Crystal fields and magnetic properties of $NdSn_3$, $NdPb_3$ and $Ndin_3$, Journal de Physique, 36: 329-33.

6. AM Van Diepen, RS Craig, WE Wallage (1971) Crystal field and magnetic heat capacity in PrIn3 and CeIn3, Journal of Physics and Chemistry of Solids, 32: 8.

7. K Satoh, Y Fujimaki, I Umehara, J Itoh, Y Ōnuki M, Low-temperature specific heat of RIn3 (R= La-Ho), Physica B: Condensed Matter, 188: 658-60.

8. MU Salma, MA Rahman (2018) Study of structural, elastic, electronic, mechanical, optical and thermodynamic properties of NdPb3 intermetallic compound: DFT based calculations, Computational Condensed Matter, 15: 42-7.

9. M Shafiq, M Yazdani- Kachoei, S Jalali-Asadabadi, I Ahmad (2017) Electric field gradient analysis of RIn3 and RSn3 compounds (R= La, Ce, Pr and Nd)," Intermetallics, 91: 95-9.

10. JP Sanchez, JM Friedt, GK Shenoy, A Percheron, JC Achard (1991) Electronic and magnetic properties of rare-earth-Sn3 compounds from 119Sn Mossbauer spectroscopy, Journal of Physics C: Solid State Phys, 9: 2207-18.

11. I Umehara, N Nagai, Y Ōnuki (1999) de Haas-van Alphen effect in PrIn3, Journal of the Physical Society of Japan, 60: 3150-3.

12. I Umehara T Ebihara, N Nagai, K Satoh, Y Fujimaki (1992) Magnetoresistance and de Haas-van Alphen effect in the antiferromagnetic compound NdIn3," Journal of the Physical Society of Japan, 61: 1633-44.

13. K Satoh, Y Fujimaki, I Umehara, J Itoh, Y Ōnuki et al. (1993) Low-temperature specific heat of RIn3 (R= La-Ho)," Physica B: Condensed Matter, 186: 658-60.

14. T Ebihara, I Umehara, AK Albessard, K Satoh, Y Ōnuki (1993) Fermi surface property of branch d in CeIn3, Physica B: Condensed Matter, 186: 123-5.

15. Y Tokura, N Nagaosa (2000) Orbital physics in transition-metal oxides, Sci, 288: 462-8.

16. E Dagotto (2005) Complexity in strongly correlated electronic systems, Sci, 309: 257-62.

17. W Suski (1999) Physics of the f-electron intermetallics," Phys. Solid State, 41: 733-7.

18. E Wigner (1934) On the interaction of electrons in metals, Phys Rev, 46: 1002-11.

19. JA Abraham, G Pagare, SS Chouhan, SP Sanyal (2014) High pressure structural, elastic, mechanical and thermal behavior of LaX3 (X= In, Sn, Tl and Pb) compounds: A FP-LAPW study, Comp. Mat. Sci, 100: 423-32.

20. RJ Gambino, NR Stemple, AM Toxen (1968) Superconductivity of lanthanum intermetallic compounds with the Cu3Au structure," J. Phys.: Chem. of solids, 29: 295-302.

21. KA Gschneidner (1964) Physical properties and interrelationships of metallic and semi metallic elements," Solid State Phys, 16: 275-426.

22. NVC Shekar, PC Sahu (2006) Pressure induced structural behavior in f-electron based AB, AB2 and AB3 intermetallics, J. Mat. Sci, 41: 3207-28.

23. S Ram, V Kanchana, A Svane, SB Dugdale, NE Christensen (2013) Fermi surface properties of AB3 (A = Y, La; B = Pb, In, Tl) intermetallic compounds under pressure, J Conden Matter, 25: 1-9.

24. SJ Asadabadi, S Cottenier, H Akbarzadeh, R Saki, M Rots (2002) Valency of rare earths in RIn3 and RSn3: Ab initio analysis of electric-field gradients, Phys Rev B, 66: 195103-13.

25. KA Gschneidner, A Russell, A Pecharsky, J Morris, Z Zhang (2003) A family of ductile intermetallic compounds," Nat. Mat, 2: 587-90.

26. S Ram, V Kanchana, G Vaitheeswaran, A Svane, SB Dugdale (2012) Electronic topological transition in LaSn3 under pressure, Phys Rev B, 85: 174531.

27. JO Choi, JY Kima, CO Choi, JK Kim, PK Rohatgi (2004) Effect of rare earth element on microstructure formation and mechanical properties of thin wall ductile iron castings, Mater. Sci. Eng. A, 383: 323-33.

28. JA Abraham, G Pagare, SP Sanyal (2015) Ab-initio calculations of structural, electronic, elastic and mechanical properties of REIn3 and RETl3 (RE= Yb & Lu) intermetallic compounds," Advans. Phys. Theories Applications, 45: 66-71.

29. W Suski (1999) Physics of the f-electron intermetallics," Phys. solid state, 41: 733-7.

30. SJ Asadabadi, S Cottenier, H Akbarzadeh, R Saki, M Rots, Valency of rare earths in RIn3 and RSn3: Ab initio analysis of electric-field gradients, Phys Rev B, 38: 1284- 7.

31. R Harris, GV Raynor (1965) Rare earth intermediate phases: I. Phases formed with tin and indium," J. Less Common Met, 1: 598-606.

32. RJ Gambino, NR Stemple, AM Toxen (1968) Superconductivity of lanthanum intermetallic compounds with the Cu3Au structure," J. Phys. Chem. Solids, 29: 295-302.

33. PC Sahu, NVC Shekar, M Yousuf, KG Rajan (1997) Implications of a pressure induced phase transition in the search for cubic Ti3Al," Phys. Rev. Lett, 78: 1054-7.

34. C Fiolhais, F Nogueira, MA Marques, Eds (2003) A Primer in Density Functional Theory, 620. Springer Science & Business Media.

35. K Burke (2012) Perspective on density functional theory," The Journal of Chemical Physics, 136: 150901.

36. E Fabiano, LA Constantin, FD Sala (2011) Exchange-correlation generalized gradient approximation for gold nanostructures," The Journal of Chemical Physics, 134: 194112-21.

37. Morrison RA (2019) Equations of State, Sound Velocities, and Thermo-elasticity of Iron-Nickel-Silicon Alloys in the Earth-'s Inner Core (Doctoral dissertation, California Institute of Technology).

38. A Gerolin, J Grossi, P Gori-Giorgi (2019) Kinetic correlation functional from the entropic regularization of the strictly correlated electrons problem, Journal of Chemical Theory and Computation, 16: 488-98.

39. P Blaha, K Schwarz, G Madsen, D Kvasnicka, J Luitz (2014) WIEN2k, An augmented plane wave plus local orbitals program for calculating crystal properties user's guide, 14.2, Vienna University of Technology, Inst. Physical & Theoretical Chem, Getreidemarkt 9/156, A-1060 Vienna, Austria.

40. Witt WC, Shires BW, Tan CW, Jankowski WJ, Pickard C.J (2021) Random Structure Searching with Orbital-Free Density Functional Theory. The Journal of Physical Chemistry A, 125: 1650-60.

41. K Schwarz, P Blaha (2003) Solid state calculations using WIEN2K," Computational Material Science, 28: 259-73.

42. HR Aliabad, M Kheirabadi (2014) Thermoelectricity and superconductivity in pure and doped Bi2Te3 with Se," Physica B: Condensed Matter, 433: 157.

43. GK Madsen, DJ Singh (2006) BoltzTraP A code for calculating band-structure dependent quantities," Comput. Phys. Commun, 175: 67.

44. CE Ekuma, DJ Singh, J Moreno, M Jarrell (2012) Optical properties of PbTe and PbSe, Physical Review B, 85: 85205-13.

45. Ali Z, Khan I, Rahman M, Ahmad R, Ahmad I (2016) Electronic structure of the LiAA′ O 6 (A=Nb, Ta, and A′= W, Mo) ceramics by modified Becke-Johnson potential. Opt. Mater, 58: 466.

46. Ali Z, Shafiq M, Asadabadi SJ, Aliabad HR, Khan I, Ahmad I (2014) Magneto-electronic studies of anti-perovskites NiNMn3 and ZnNMn3. Comput. Mater. Sci, 81: 141.

47. Wang Z, Moosavi SH, Kroener M, Woias P (2015) Development of a Thermoelectric Nanowire Characterization Platform (TNCP) for Structural and Thermoelectric Investigation of Single Nanowires. Thermoelectric Bi2Te3 Nanomaterials.

48. Aliabad HR, Ghazanfari M, Ahmad I, Saeed M (2012) Ab initio calculations of structural, optical and thermoelectric properties for CoSb 3 and ACo 4 Sb 12 (A= La, Tl and Y) compounds. Comput. Mater. Sci, 65: 509.

49. JN Hausmann, M Oudah, A Ikeda, S Yonezawa, Y Maeno (2018) Controlled synthesis of the antiperovskite oxide superconductor Sr3-xSnO," Superconductor Science and Technology, 31: 055012-8.

50. X. Yuan et al. (2021) Design of negative/nearly zero thermal expansion behavior over a wide temperature range by multiphase composite," Materials & Design, 203: 109591-601.

51. H Yamamoto, T Imai, Y Sakai, M Azuma (2018) Colossal negative thermal expansion in electron-doped ABX tetragonal, Angewandte Chemie International Edition, vol. 57: 8170-3.

52. Janesko BG, Verma P, Scalmani G, Frisch MJ, Truhlar DG (2020) M11plus, a range-separated hybrid meta functional incorporating nonlocal rung-3.5 correlation, exhibits broad accuracy on diverse databases. The journal of physical chemistry letters, 11: 3045- 50.

53. Rabin, Y-M Lin, MS Dresselhaus (2001) Anomalously high thermoelectric figure of merit in Bi1-xSbx nanowires by carrier pocket alignment," Applied Physics Letters, 79: 2001.

54. Feng Y, Zhang J, Qin P, Liu S, Yang Q et al. (2019) Characterization of elevated-temperature high strength and decent thermal conductivity extruded Mg-Er-Y-Zn alloy containing Nano-spaced stacking faults. Materials Characterization, 155: 109823-34.

55. AH Sofi, MA Shah (2010) Structural and electrical properties of copper doped In2O3 nanostructures prepared by citrate gel processes," Materials Research Express, vol. 6: 45039-45047.

56. H. Hardianto (2020) Textile-Based Thermoelectric Generators Based on Conductive Yarns, Doctoral dissertation, Ghent University.

57. KA Moltved, KP Kepp (2019) The Metal Hydride Problem of Computational Chemistry: Origins and Consequences," The Journal of Physical Chemistry A, 123: 2888-900.